IUST
Iran University of Science and Technology

Iranian Journal of Electrical and Electronic Engineering

Journal Homepage: ijeee.iust.ac.ir

Research Paper

Model Predictive Control of a BCDFIG With Active and Reactive Power Control Capability for Grid-Connected Applications

R. Rezavandi*, D. A. Khaburi*(C.A.), M. Siami*, M. Khosravi*, and S. Heshmatian*

Abstract: Recently, Brushless Cascaded Doubly Fed Induction Generator (BCDFIG) has been considered as an attractive choice for grid-connected applications due to its high controllability and reliability. In this paper, a Finite Control Set Model Predictive Control (FCS-MPC) method with active and reactive power control capability in grid-connected mode is proposed for controlling the BCDFIG in a way that notable improvement of the dynamic response, ripple reduction of the active and reactive power waveforms and also better THD performance are achieved compared to the traditional approaches such as Vector Control (VC) method. For this purpose, the required mathematical equations are obtained and presented in detail. In order to validate the proposed method performance, a 1–MW grid-connected BCDFIG is simulated in MATLAB/Simulink environment.

Keywords: Brushless Cascaded Doubly Fed Induction Generator (BCDFIG), Dynamic Response, Predictive Control, Grid-Connected Systems.

Nomenclature

Variables

v, i, λ	Voltage, current and flux
ω_{PM},ω_{CM},ω_m	Electrical angular frequencies of the power machine, control machine and rotor
ω_c, ω_r	Control machine and rotor angular frequencies (relative to the synchronous reference frame)
R, L	Resistance and inductance
P, Q	Active and reactive powers
T_s	Sampling time

Subscripts and Superscripts

sp, *sc*, *r*	Power machine stator, control machine stator and rotor
l, *mp*, *mc*	Leakage inductance, rotor and power machine mutual inductance, rotor and control machine mutual inductance
d, *q*	d-q rotating frame

Iranian Journal of Electrical and Electronic Engineering, 2021.
Paper first received 12 January 2019, revised 01 August 2020, and accepted 03 August 2020.
* The authors are with the Electrical Engineering Department, Iran University of Science and Technology (IUST), Tehran, Iran.
E-mails: ramtinrzs@elec.iust.ac.ir, khaburi@iust.ac.ir, siami@iust.ac.ir, mkhosravi@elec.iust.ac.ir, and saeed_heshmatian@elec.iust.ac.ir.
Corresponding Author: D. A. Khaburi.
https://doi.org/10.22068/IJEEE.17.2.1422

1 Introduction

DURING the recent decades, several types of generators have been used in grid-connected Wind Energy Conversion Systems (WECS), among which, Doubly-Fed Induction Generator (DFIG) is dominant in the current market because of its several benefits such as elimination of the need for employing full-scale power converters [1, 2]. Nevertheless, DFIG needs regular maintenance due to the existence of slip rings and brushes which in turn, leads to low reliability and extra cost [3].

In order to overcome the aforementioned drawback of DFIGs, the Brushless Doubly-Fed Induction Generator (BDFIG) has been employed in literature as an attractive solution [4-6]. In BDFIGs, slip rings and brushes are eliminated. Therefore, the reliability of this generator is improved significantly. Also, in case of a fault occurrence at the grid-side, BDFIG will have a more satisfactory performance. Moreover, Brushless Cascaded Doubly-Fed Induction Generator

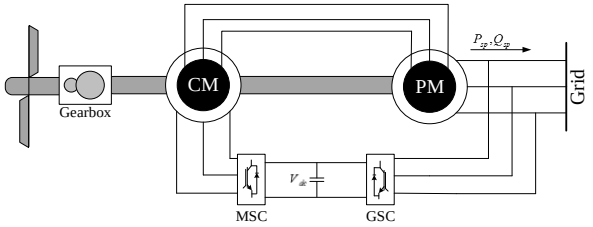

Fig. 1 Schematic diagram of BCDFIG.

(BCDFIG) [7] (Fig. 1) is a special variation of BDFIG in which two separate machines, named Power and Control Machines (PM and CM), are employed instead of using two stator windings with different pole numbers in one frame. The PM and CM rotors are coupled mechanically and electrically in this structure. The operating principles of BDFIGs and BCDFIGs are almost the same. However, the BCDFIG is usually studied in different research works in sake of simplicity.

Controllability of active and reactive powers is a major advantage of DFIGs which is also achievable with BDFIGs [3], [8-9]. Different research works have been conducted in order to address the active and reactive power control of BDFIGs, including open-loop control [10], phase-angle control [11], closed-loop frequency control [12], and finally the well-known Vector Control (VC) method [13, 14]. In the VC method, which is the most general control strategy and also known as Voltage Oriented Control (VOC), both the active and reactive powers are controlled independently by regulating the current components in the d-q reference frame using PI current controllers. However, this method needs employing suitable rotary transformation techniques and a notable tuning effort for the several PI controllers in order to achieve wide-range system stability. Several efforts have been made in order to improve the VC method performance. In [15], an improved Direct Voltage Control (DVC) is proposed for BDFIG based on the traditional vector control scheme. The proposed method performance is simple, robust and cost-effective. In [16], an improved vector control method is proposed based on Proportional Integral Resonant (PI+R) controller in order to enhance the stability and robustness in case of parameter uncertainties and unbalanced grid conditions.
On the other hand, Direct Torque Control (DTC) and Direct Power Control (DPC) strategies are also employed for controlling BDFIGs in order to get rid of the notable tuning effort and also the relative complexity of vector control strategy [17-18]. In comparison to the VC strategy, DPC directly controls the active and reactive powers instead of the AC current components, by employing a predefined switching table. This method results in great dynamic responses. Moreover, some variations are also proposed in order to add some capabilities to the conventional DTC. For example, in [5], the DTC method is modified in a way that smooth synchronization is also achieved. However, it should be considered that the actuation vector chosen in the DTC/DPC strategies will not always be the optimal one and hence, employing these methods could result in notable ripples in torque/power waveforms.

Predictive control is an advanced control technique that is widely applied to machine drives and power electronic converters recently [19-20]. The predictive approach controls the system based on minimizing a cost function which consists of future values of different system variables. A model of the system is employed in order to predict the future behavior of the system. This strategy has been successfully applied to DFIGs, resulting in excellent dynamic and steady state responses and at the same time, decreasing the number of linear PI controllers and also the challenging parameter tuning effort. In [21], A Predictive Direct Power Control (P-DPC) scheme is applied to a DFIG which directly controls the active and reactive powers by defining a cost function including these two power components. Moreover, another variation is presented in [22] in order to reduce the computational burden by using the switching states of the rotor-side converter as control inputs. However, despite the several advantages of the MPC method and its successful implementation for DFIGs, this method has not been adapted to be used with BCDFIGs.

In this paper, the BCDFIG model equations that are required to implement MPC, are developed for current control of this machine. The MPC algorithm is proposed based on these equations. Next, the algorithm is adapted in a way that active and reactive powers are controllable for grid-connected WECS applications. The VC and proposed MPC methods are simulated in MATLAB/Simulink software and the performance and effectiveness of the proposed method is validated and compared with the VC from different aspects such as transient and steady state responses.

2 BCDFIG Modeling

As mentioned earlier, BCDFIG consists of two separate machines. The rotors of these machines are coupled both mechanically and electrically so that their rotating magnetic fields are identical. The BCDFIG model in d-q synchronous reference frame is described by the following equations [23]:

$$V_{sp}^{q} = R_{sp} i_{sp}^{q} + \frac{d\lambda_{sp}^{q}}{dt} + \omega_{PM} \lambda_{sp}^{d} \tag{1}$$

$$V_{sp}^{d} = R_{sp} i_{sp}^{d} + \frac{d\lambda_{sp}^{d}}{dt} - \omega_{PM} \lambda_{sp}^{q} \tag{2}$$

$$V_{sc}^{q} = R_{sc} i_{sc}^{q} + \frac{d\lambda_{sc}^{q}}{dt} + \omega_{c} \lambda_{sc}^{d} \tag{3}$$

$$V_{sc}^{d} = R_{sc} i_{sc}^{d} + \frac{d\lambda_{sc}^{d}}{dt} - \omega_{c} \lambda_{sc}^{q} \tag{4}$$

$$0 = R_r i_r^q + \frac{d\lambda_r^q}{dt} + \omega_r \lambda_r^d \quad (5)$$

$$0 = R_r i_r^d + \frac{d\lambda_r^d}{dt} - \omega_r \lambda_r^q \quad (6)$$

$$\lambda_{sp}^{dq} = L_{lp} i_{sp}^{dq} + L_{mp}(i_{sp}^{dq} + i_r^{dq}) \quad (7)$$

$$\lambda_{sc}^{dq} = L_{lc} i_{sc}^{dq} + L_{mc}(i_{sc}^{dq} - i_r^{dq}) \quad (8)$$

$$\lambda_r^{dq} = L_{lr} i_r^{dq} + L_{mp}(i_r^{dq} + i_{sp}^{dq}) + L_{mc}(i_r^{dq} - i_{sc}^{dq}) \quad (9)$$

Note that in (5) and (6), the rotor voltage values in d and q axes have been considered as zero since the rotor terminals are short-circuit. Also, the values of ω_c and ω_r are defined as (10) and (11):

$$\omega_c = \omega_{PM} - (p_{PM} + p_{CM})\omega_m \quad (10)$$

$$\omega_r = \omega_{PM} - (p_{PM})\omega_m \quad (11)$$

Based on (1)-(11), the dynamic equivalent circuit of BCDFIG in the d-q rotating reference frame, which is shown in Fig. 2, can be obtained.

3 Vector Control Method

As mentioned earlier, vector control method is the most well-known strategy used for controlling BCDFIGs. Therefore, it is briefly discussed here and its performance is compared with the proposed method in the next sections. The basic operating principle of this strategy is based on decoupled control of the current components in order to independently control two different variables such as active and reactive powers. To implement this method for BCDFIGs, the reference of the d- and q-axis current components are calculated based on the reference values of the active and reactive powers as the first step. For this purpose, the entire PM stator flux is assumed to be in the direction of d-axis:

$$\lambda_{sp}^d = \left|\lambda_{sp}\right| \quad (12)$$

$$\lambda_{sp}^q = 0 \quad (13)$$

According to (12) and (13), and considering that the generator is connected to a stiff grid (a grid with fixed voltage amplitude and frequency), the reference values of the active and reactive powers are obtained using the following equations:

$$P_{sp} = \frac{3}{2}(V_{sp}^q i_{sp}^q) \quad (14)$$

$$Q_{sp} = \frac{3}{2}(V_{sp}^q i_{sp}^d) \quad (15)$$

Next, the reference values of the CM current components are achieved using two PI controllers and the errors of PM current components. The CM voltage references are then determined using two other PI controllers and based on the errors of CM current components. Finally, the Machine Side Converter (MSC) is controlled such that these reference voltages are applied to the CM. The entire block diagram of this control scheme is depicted in Fig. 3, in which, the decoupling blocks are responsible for compensating interconnected dynamics [23].

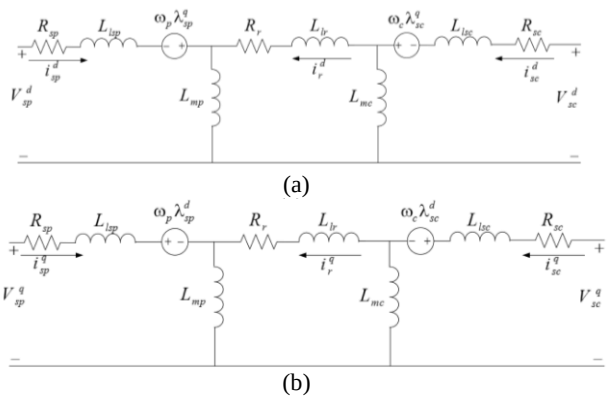

Fig. 2 Dynamic equivalent circuit of BCDFIG; a) q-axis, b) d-axis.

4 Proposed Finite Control Set Model Predictive Control Method

As stated earlier, Model Predictive Control (MPC) strategy is an advanced control method which could be further categorized into Continuous Control Set (CCS) and Finite Control Set (FCS) MPC [24]. Because of the discrete nature of power electronics converters, the FCS-MPC could be easily employed with them. The FCS-MPC operating principle is based on the prediction of machine future states using an appropriate discretized machine model. The values of different variables such as currents, voltages, speed, and etc., which are required in the prediction model, could be measured. Then, these predicted values are used in a predefined cost function. Finally, the switching state (voltage vector) which minimizes the cost function value will be selected as the best actuation to be applied to the MSC. For applying FCS-MPC to BCDFIG, the equations which directly relate the CM d- and q-axis stator voltages to the CM d- and q-axis stator currents must be obtained. In this section, these equations are determined and then the proposed algorithm operating principles will be explained.

4.1 Development of the Prediction Model

By using (8) in (3) and (4), the following equations could be obtained:

$$V_{sc}^q = R_{sc} i_{sc}^q + L_{sc}\frac{di_{sc}^q}{dt} - L_{mc}\frac{di_r^q}{dt} + \omega_c L_{sc} i_{sc}^d - \omega_c L_{mc} i_r^d \quad (16)$$

$$V_{sc}^d = R_{sc} i_{sc}^d + L_{sc}\frac{di_{sc}^d}{dt} - L_{mc}\frac{di_r^d}{dt} - \omega_c L_{sc} i_{sc}^q + \omega_c L_{mc} i_r^q \quad (17)$$

where $L_{sc} = L_{lsc} + L_{mc}$.

The problem with the above equations is existence of

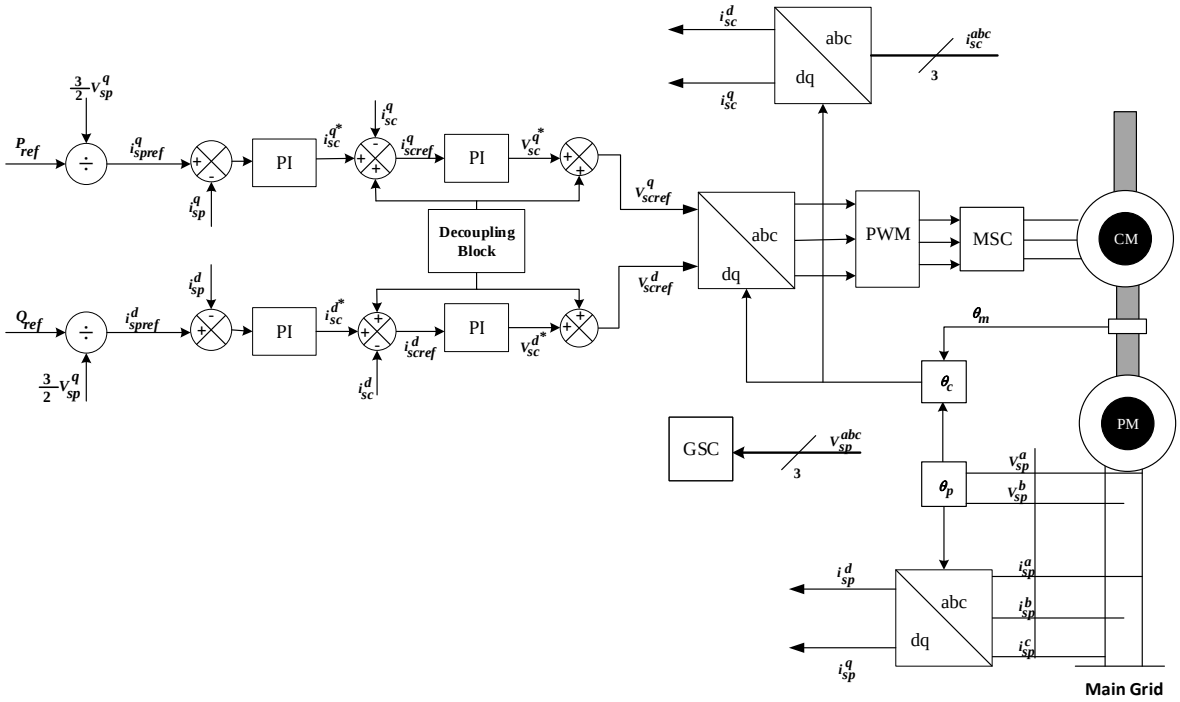

Fig. 3 Implementation block diagram of the vector control for BCDFIG.

the terms representing the rotor currents. Since these currents are not measureable, they must be replaced with measureable quantities using the machine model equations. According to (9), the rotor current in d-q reference frame is as follows:

$$i_r^{dq} = \frac{\lambda_r^{dq} - L_{mp} i_{sp}^{dq} + L_{mc} i_{sc}^{dq}}{L_r} \tag{18}$$

where $L_r = L_{lr} + L_{mc} + L_{mp}$.

Since the derivation of the rotor current term is available in (16) and (17), the derivative from of (18) is also needed:

$$L_r \frac{di_r^{dq}}{dt} = \frac{d\lambda_r^{dq}}{dt} - L_{mp} \frac{di_{sp}^{dq}}{dt} + L_{mc} \frac{di_{sc}^{dq}}{dt} \tag{19}$$

To predict the behavior of the d- and q-axis currents for different voltage vectors, all the derivative terms must be eliminated except the derivation of CM current components. In the other words, the terms representing derivation of the rotor flux and the PM stator currents must be omitted. The derivation of (7) is:

$$\frac{di_{sp}^{dq}}{dt} = \frac{\frac{d\lambda_{sp}^{dq}}{dt} - L_{mp} \frac{di_r^{dq}}{dt}}{L_{sp}} \tag{20}$$

where $L_{sp} = L_{lsp} + L_{mp}$.

Also, the following equations can be obtained by rearranging (5) and (6):

$$\frac{d\lambda_r^d}{dt} = -R_r i_r^d + \omega_r \lambda_r^q \tag{21}$$

$$\frac{d\lambda_r^q}{dt} = -R_r i_r^q - \omega_r \lambda_r^d \tag{22}$$

By substituting (20)-(22) into (19), the following equations are obtained:

$$L_r \frac{di_r^d}{dt} = -R_r i_r^d + \omega_r \lambda_r^q - L_{mp} \left(\frac{\frac{d\lambda_{sp}^d}{dt} - L_{mp} \frac{di_r^d}{dt}}{L_{sp}} \right) + L_{mc} \frac{di_{sc}^d}{dt} \tag{23}$$

$$L_r \frac{di_r^q}{dt} = -R_r i_r^q - \omega_r \lambda_r^d - L_{mp} \left(\frac{\frac{d\lambda_{sp}^q}{dt} - L_{mp} \frac{di_r^q}{dt}}{L_{sp}} \right) + L_{mc} \frac{di_{sc}^q}{dt} \tag{24}$$

The above equations can be simplified as follows:

$$\frac{di_r^d}{dt} = -\frac{R_r}{A} i_r^d + \omega_r \frac{\lambda_r^q}{A} - \frac{L_{mp}}{L_{sp} A} \frac{d\lambda_{sp}^d}{dt} + \frac{L_{mc}}{A} \frac{di_{sc}^d}{dt} \tag{25}$$

$$\frac{di_r^q}{dt} = -\frac{R_r}{A} i_r^q - \omega_r \frac{\lambda_r^d}{A} - \frac{L_{mp}}{L_{sp} A} \frac{d\lambda_{sp}^q}{dt} + \frac{L_{mc}}{A} \frac{di_{sc}^q}{dt} \tag{26}$$

where $A = L_r - L^2_{mp}/L_{sp}$.

In (25) and (26), there still exists two undesired terms. These two terms are the PM stator flux and the rotor current derivations that must be removed. It should be noted that the equation used for eliminating the rotor current was already obtained in (18). For omission of the PM stator flux derivation, (1) and (2) could be used:

$$\frac{d\lambda_{sp}^q}{dt} = V_{sp}^q - R_{sp} i_{sp}^q - \omega_p \lambda_{sp}^d \tag{27}$$

$$\frac{d\lambda_{sp}^{d}}{dt} = V_{sp}^{d} - R_{sp} i_{sp}^{d} + \omega_p \lambda_{sp}^{q} \tag{28}$$

By employing (18), (27), and (28), the final equations for the rotor current derivations are as follows:

$$\frac{di_r^d}{dt} = -\frac{R_r}{A}\left(\frac{\lambda_r^d - L_{mp} i_{sp}^d + L_{mc} i_{sc}^d}{L_r}\right) + \omega_r \frac{\lambda_r^q}{A} - \frac{L_{mp}}{L_{sp} A}\left(V_{sp}^d - R_{sp} i_{sp}^d + \omega_p \lambda_{sp}^q\right) + \frac{L_{mc}}{A}\frac{di_{sc}^d}{dt} \tag{29}$$

$$\frac{di_r^q}{dt} = -\frac{R_r}{A}\left(\frac{\lambda_r^q - L_{mp} i_{sp}^q + L_{mc} i_{sc}^q}{L_r}\right) - \omega_r \frac{\lambda_r^d}{A} - \frac{L_{mp}}{L_{sp} A}\left(V_{sp}^q - R_{sp} i_{sp}^q - \omega_p \lambda_{sp}^d\right) + \frac{L_{mc}}{A}\frac{di_{sc}^d}{dt} \tag{30}$$

By substituting (29) and (30) in (16) and (17) and rearranging them, the CM stator voltages are obtained based on only measurable quantities:

$$\frac{V_{sc}^d}{R_{sc}} = j_1 \frac{di_{sc}^d}{dt} + j_2 i_{sc}^d + j_3 i_{sc}^q + j_4 \lambda_r^q + j_5 \lambda_r^d + j_6 i_{sp}^q + (j_7 + j_8) i_{sp}^d + j_9 \lambda_{sp}^q + j_{10} V_{sp}^d \tag{31}$$

$$\frac{V_{sc}^q}{R_{sc}} = j_1 \frac{di_{sc}^q}{dt} + j_2 i_{sc}^q - j_3 i_{sc}^d - j_4 \lambda_r^d + j_5 \lambda_r^q - j_6 i_{sp}^d + (j_7 + j_8) i_{sp}^q - j_9 \lambda_{sp}^d + j_{10} V_{sp}^q \tag{32}$$

where the constant coefficients j_1 to j_{10} are defined as follows:

$$j_1 = \tau_{sc} - \frac{L_{mc}^2}{A R_{sc}},\quad j_2 = 1 + \frac{R_r L_{mc}^2}{R_{sc} L_r A},\quad j_3 = \omega_c\left(\frac{L_{mc}^2}{R_{sc} L_r} - \tau_{sc}\right),$$

$$j_4 = \left(\frac{\omega_c L_{mc}}{R_{sc} L_r} - \frac{\omega_r L_{mc}}{R_{sc} A}\right),\quad j_5 = \frac{R_r L_{mc}}{R_{sc} L_r A},\quad j_6 = \frac{-\omega_c L_{mc} L_{mp}}{R_{sc} L_r},$$

$$j_7 = -\left(\frac{R_r L_{mp} L_{mc}}{R_{sc} L_r A}\right),\quad j_8 = -\left(\frac{R_{sp} L_{mp} L_{mc}}{R_{sc} L_{sp} A}\right),\quad j_9 = \frac{\omega_c L_{mc} L_{mp}}{A R_{sc} L_{sp}},$$

$$j_{10} = \frac{L_{mc} L_{mp}}{A R_{sc} L_{sp}}.$$

Moreover, $\tau_{sc} = R_{sc}/L_{sc}$ is the time constant of the CM stator.

Next, forward Euler's approximation is employed in order to discretize the derivations of the CM current components in (31) and (32) over one sampling time *Ts*. By rearranging the obtained discrete equations, the following equations are resulted and used for one step prediction of the CM stator currents in d- and q-axis:

$$i_{sc}^d(k+1) = \frac{T_s}{j_1}\left[\frac{V_{sc}^d(k)}{R_{sc}} + \left(\frac{j_1}{T_s} - j_2\right) i_{sc}^d(k) - j_3 i_{sc}^q(k) - j_4 \lambda_r^q(k) - j_5 \lambda_r^d(k) - j_6 i_{sp}^q(k) - (j_7 + j_8) i_{sp}^d(k) - j_9 \lambda_{sp}^q(k) - j_{10} V_{sp}^d(k)\right] \tag{33}$$

$$i_{sc}^q(k+1) = \frac{T_s}{j_1}\left[\frac{V_{sc}^q(k)}{R_{sc}} + \left(\frac{j_1}{T_s} - j_2\right) i_{sc}^q(k) + j_3 i_{sc}^d(k) + j_4 \lambda_r^d(k) - j_5 \lambda_r^q(k) + j_6 i_{sp}^d(k) - (j_7 + j_8) i_{sp}^q(k) + j_9 \lambda_{sp}^d(k) - j_{10} V_{sp}^q(k)\right] \tag{34}$$

In (33) and (34), the voltage and current values of the PM and CM stators can be easily measured. However, different fluxes are also available in these equations. The two following equations, which are easily obtained from the described model, can be used to calculate their values at instance *k*:

$$\lambda_{sp}^d(k) = \left(V_{sp}^d(k) - R_{sp} i_{sp}^d(k) + \omega_{PM} \lambda_{sp}^q(k-1)\right) T_s + \lambda_{sp}^d(k-1) \tag{35}$$

$$\lambda_{sp}^q(k) = \left(V_{sp}^q(k) - R_{sp} i_{sp}^q(k) - \omega_{PM} \lambda_{sp}^d(k-1)\right) T_s + \lambda_{sp}^q(k-1) \tag{36}$$

$$\lambda_r^{dq}(k) = \frac{L_r}{L_{mp}} \lambda_{sp}^{dq}(k) + \frac{L_{mp}^2 - L_{sp} L_r}{L_{mp}} i_{sp}^{dq}(k) - L_{mc} i_{sc}^{dq}(k) \tag{37}$$

4.2 Cost Function Definition and Operating Principles of the Proposed Algorithm

As discussed earlier, the optimal switching state which is applied to the converter at the upcoming sample, is selected based on minimizing the value of a predefined cost function. This cost function contains the different control objectives. Based on the model developed above, the CM currents are chosen as the control goals here. Therefore, the Cost Function (CF) is defined as below:

$$g = \left(i_{sc\_ref}^q(k+1) - i_{sc}^q(k+1)\right) + \left(i_{sc\_ref}^d(k+1) - i_{sc}^d(k+1)\right) \tag{38}$$

In (38), $i_{sc\_ref}^q(k+1)$ and $i_{sc\_ref}^d(k+1)$ are the reference values of the CM current components which are generated by external controllers. As the grid-connected WECS application is studied in this paper, the final goal is to control the grid-side active and reactive powers and hence, the basic proposed MPC method which is formulated for controlling the CM currents should be adapted. For this purpose, the PM reference currents are calculated as the first step based on the active and reactive power references by using Eqs. (14) and (15). Next, these reference values are compared with the measured PM stator currents and the reference CM stator currents will be generated using two PI controllers. Moreover, the terms $i_{sc}^q(k+1)$ and $i_{sc}^d(k+1)$ which represent the predicted values of the CM current are calculated using (33) and (34). It should

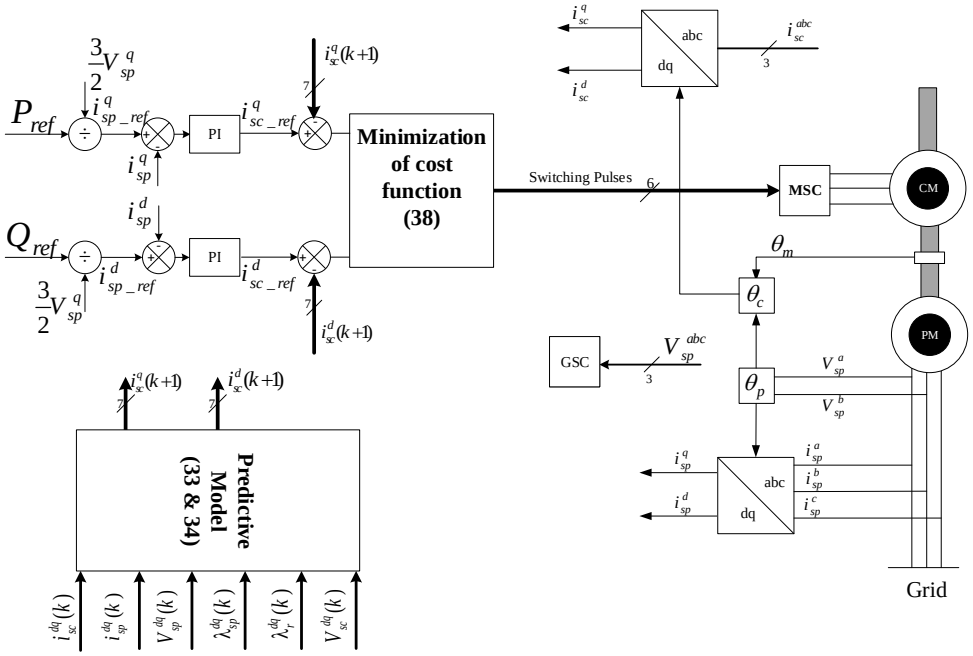

Fig. 4 Proposed control scheme block diagram.

be noted that as these two control variables have the same unit and are from the same kind, and also neither of them have more control importance than the other, the weighting factor value has selected to be one. The overall block diagram of the proposed control method is shown in Fig. 4.

As the 2-Level Voltage Source Inverter (2L-VSI) is employed as the MSC, only 8 different switching states (including 6 active vectors and 2 zero voltage vectors) should be evaluated [25]. The state that minimizes the CF value is chosen as the appropriate switching vector and will be applied to the MSC in the next time interval.

5 Simulation Results and Discussion

In order to validate the satisfactory performance and also the advantages of the proposed control method, the systems shown in Figs. 3 and 4 are simulated using the MATLAB/Simulink software. For implementing both vector control and the proposed MPC strategies, a 1-MW BCDFIG is considered. The parameters used in the simulation are given in Table. 1. It should be noted that the average switching frequency of the vector control and proposed MPC methods are 4167 and 4247 Hz, respectively. Also, the value of the limited prediction horizon is one in the proposed method. Moreover, the reference values for active and reactive powers during the simulation time are considered the same for both methods and shown in Table 2.

The CM stator currents for the both control methods are depicted in Fig. 5. The amplitude and frequency of the reference CM stator currents are such that the active and reactive power reference values could be reached at the steady-state condition. According to this figure, both strategies represent satisfactory performances in terms

Table 1 BCDFIG parameters.

Parameters	BCDFIG	
	PM	CM
R_s [mΩ]	3.654	8
R_r [mΩ]	3.569	6
L_{ls} [mH]	0.1304	0.144
L_{lr} [mH]	0.1198	0.145
L_m [mH]	4.12	5.2
Poles	4	6
P_n [MW]	1	0.5
V_n [V]	575	575

Table 2 Reference values for active and reactive powers.

Reference N.O.	**Time [**sec**]**	**P [**MW**]**	Q **[**kVA**r]**
1	0-8	-0.5	+50
2	8-16	-0.2	-50
3	16-25	-0.8	0

of tracking the CM stator current references in all conditions. However, it is seen that the waveforms are smoother in the proposed method and the current distortions available in the VC method have decreased. Fig. 6 demonstrates the PM stator currents. The reference waveforms for these currents are determined based on the desired active and reactive powers. The amplitude of these references are about 0.5, 0.2, and 0.8 amperes for references 1, 2, and 3, respectively. According to Fig. 6, both simulated methods provide a satisfactory performance in terms of tracking the reference waveforms. For better comparison, the THD values of the PM and CM currents have been compared for both methods in Figs. 7(a) and 7(b), respectively.

Moreover, the active and reactive power exchanged with the grid in both VC and proposed methods, have been shown in Figs. 8 and 9, respectively. According to

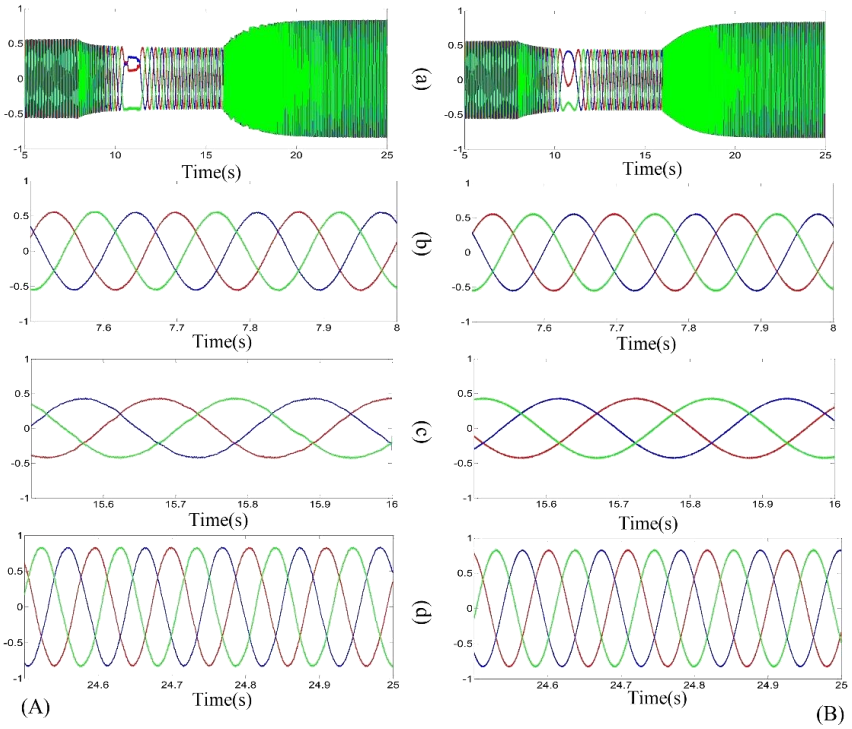

Fig. 5 Three-phase stator currents of CM for A) vector control and B) proposed strategies; a) Reference waveforms, b) Steady-state current during the application of reference 1, c) Steady-state current during the application of reference 2, and d) Steady-state current during the application of reference 3.

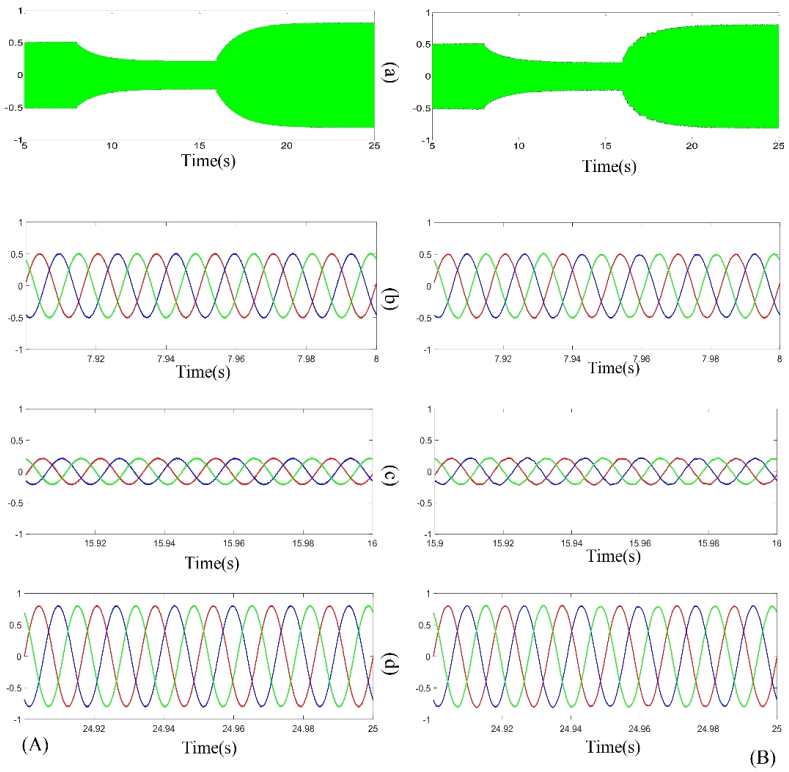

Fig. 6 Three-phase stator currents of PM for A) vector control and B) proposed strategies; a) Reference waveforms, b) Steady-state current during the application of reference 1, c) Steady-state current during the application of reference 2, and d) Steady-state current during the application of reference 3.

(a) (b)

Fig. 7 THD values of the steady-state: a) PM and b) CM stator currents for VC and proposed methods.

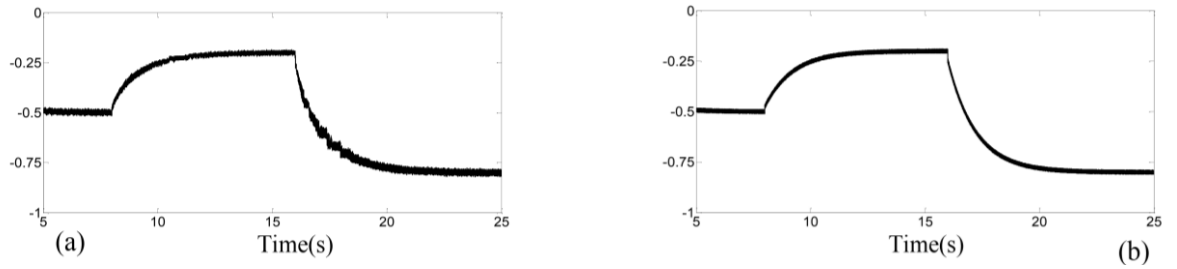

Fig. 8 Power machine active power (MW); a) Vector control andb) proposed MPC method.

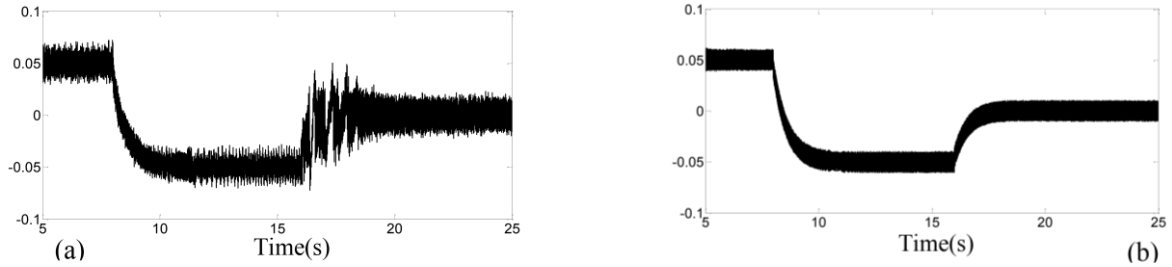

Fig. 9 Power machine reactive power (MVAr); a) Vector control and b) proposed MPC method.

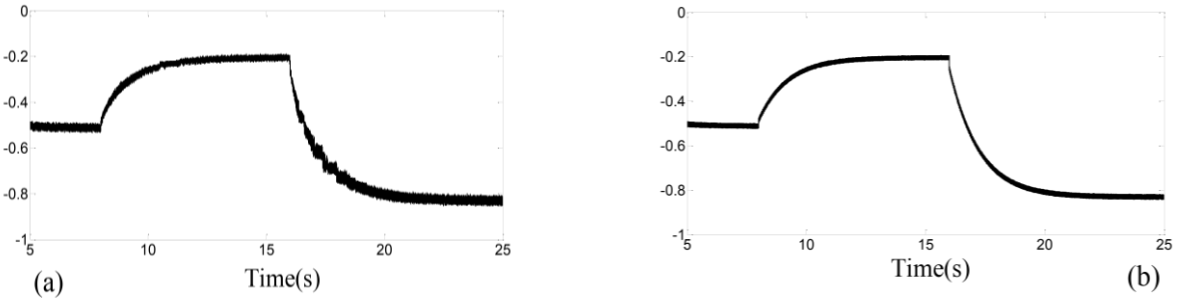

Fig. 10 BCDFIG electromagnetic torque (p.u): a) Vector control and b) proposed MPC method.

these figures, the reference values are tracked appropriately in both methods. Also, it can be observed that in the proposed MPC method, the transient-state distortions of these two quantities have considerably decreased compared to the VC method. Diminution of distortions could be especially observed in the transient time interval of t = 16-19 s. The BCDFIG electromagnetic torque value varies with the change of the mechanical torque applied to the rotor which in turn, is resulted from the variation of reference values. The generator reaches the steady-state condition when these two torques are in a balanced condition. The BCDFIG electromagnetic torque waveforms are shown in Fig. 10. The distortions of the torque waveform are diminished by the MPC method like those of the active and reactive powers. The THD values of the torque and also steady-state active power waveforms for the VC and proposed methods are depicted in Figs. 11(a) and 11(b), respectively. According to this figure, the ripple percentages have been improved for all the references by employing the proposed method.

5 Conclusion

In this paper, a novel MPC strategy has been proposed in order to control the active and reactive power

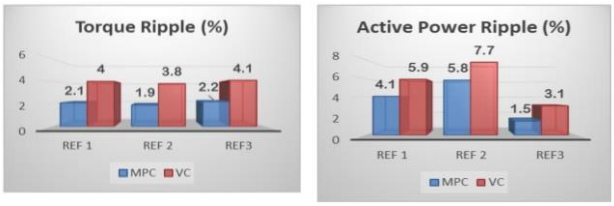

(a) (b)

Fig. 11 Ripple percentage values of a) the electromagnetic torque and (b) steady-state active power waveforms for VC and proposed methods.

exchange of BCDFIG with the grid. For this purpose, the BCDFIG model equations have been adapted in a way that the proposed MPC scheme could be established. The obtained simulation results for the proposed and also the VC method reveal that the MPC method has several advantages such as improvement of the transient state responses, removal of the second two PI blocks available in the vector control method, and ripple reduction of the active and reactive power waveforms and also better THD performance compared to the traditional VC approach. These advantages, along with the benefits of BCDFIG itself, make this kind of generator a highly attractive choice to be used in WECS applications.

References

[1] H. Misra, A. Gundavarapu, and A. K. Jain, "Control scheme for DC voltage regulation of stand-alone DFIG-DC system," *IEEE Transactions on Industrial Electronics*, Vol. 64, No. 4, pp. 2700–2708, 2017.

[2] G. Rashid and M. H. Ali, "Fault ride through capability improvement of DFIG based wind farm by fuzzy logic controlled parallel resonance fault current limiter," *Electric Power Systems Research*, Vol. 146, pp. 1–8, 2017.

[3] I. Gowaid, A. S. Abdel-Khalik, A. M. Massoud, and S. Ahmed, "Ride-Through capability of grid-connected brushless cascade DFIG wind turbines in faulty grid conditions—a comparative study," *IEEE Transactions on Sustainable Ener*gy, Vol. 4, No. 4, pp. 1002–1015, 2013.

[4] M. Gholizadeh, A. Oraee, S. Tohidi, H. Oraee, and R. A. McMahon, "An analytical study for low voltage ride through of the brushless doubly-fed induction generator during asymmetrical voltage dips," *Renewable Energy*, Vol. 115, pp. 64–75, 2018.

[5] R. Sadeghi, S. M. Madani, and M. Ataei, "A new smooth synchronization of brushless doubly-fed induction generator by applying a proposed machine model," *IEEE Transactions on Sustainable Energy*, Vol. 9, No. 1, pp. 371–380, 2018.

[6] M. Gholizadeh, S. Tohidi, A. Oraee, and H. Oraee, "Appropriate crowbar protection for improvement of brushless DFIG LVRT during asymmetrical voltage dips," In*ternational Journal of Electrical Power & Energy Systems*, Vol. 95, pp. 1–10, 2018.

[7] M. El Achkar, R. Mbayed, G. Salloum, S. Le Ballois, and E. Monmasson, "Generic study of the power capability of a cascaded doubly fed induction machine," *International Journal of Electrical Power & Energy Systems*, Vol. 86, pp. 61–70, 2017.

[8] J. Hu, H. Nian, B. Hu, Y. He, and Z. Zhu, "Direct active and reactive power regulation of DFIG using sliding-mode control approach," *IEEE Transactions on Energy Conversion*, Vol. 25, No. 4, pp. 1028–1039, 2010.

[9] S. Shao, E. Abdi, F. Barati, and R. McMahon, "Stator-flux-oriented vector control for brushless doubly fed induction generator," *IEEE Transactions on Industrial Electronics*, Vol. 56, No. 10, pp. 4220–4228, 2009.

[10] D. Feng, P. Roberts, and R. McMahon, "Control study on starting of BDFM," in *IEEE Proceedings of the 41st International Universities Power Engineering Conference*, Vol. 2, pp. 660–664, 2006.

[11] S. Shao, E. Abdi, and R. McMahon, "Stable operation of the brushless doubly-fed machine (BDFM)," in *7th International Conference on Power Electronics and Drive Systems (PEDS'07)*, pp. 897–902, 2007.

[12] R. Li, R. Spee, A. K. Wallace, and G. Alexander, "Synchronous drive performance of brushless doubly-fed motors," *IEEE Transactions on Industry Applications*, Vol. 30, No. 4, pp. 963–970, 1994.

[13] D. Zhou and R. Spee, "Synchronous frame model and decoupled control development for doubly-fed machines," in *25th Annual Power Electronics Specialists Conference (PESC'94)*, Vol. 2, pp. 1229–1236, 1994.

[14] X. Chen, Z. Wei, X. Gao, C. Ye, and X. Wang, "Research of voltage amplitude fluctuation and compensation for wound rotor brushless doubly-fed machine," *Diesel Engine*, Vol. 13, p. 21, 2015.

[15] X. Wei, M. Cheng, W. Wang, P. Han, and R. Luo, "Direct voltage control of dual-stator brushless doubly fed induction generator for stand-alone wind energy conversion systems," *IEEE Transactions on Magnetics*, Vol. 52, No. 7, pp. 1–4, 2016.

[16] J. Chen, W. Zhang, B. Chen, and Y. Ma, "Improved vector control of brushless doubly fed induction generator under unbalanced grid conditions for offshore wind power generation," *IEEE Transactions on Energy Conversion*, Vol. 31, No. 1, pp. 293–302, 2016.

[17] I. Sarasola, J. Poza, M. A. Rodriguez, and G. Abad, "Direct torque control design and experimental evaluation for the brushless doubly fed machine," *Energy Conversion and Management*, Vol. 52, No. 2, pp. 1226–1234, 2011.

[18] J. Hu, J. Zhu, and D. G. Dorrell, "A new control method of cascaded brushless doubly fed induction generators using direct power control," *IEEE Transactions on Energy Conversion*, Vol. 29, No. 3, pp. 771–779, 2014.

[19] X. Wei, M. Cheng, P. Han, W. Wang, and R. Luo, "Comparison of control strategies for a novel dual-stator brushless doubly-fed induction generator in wind energy applications," in *18th International Conference on Electrical Machines and Systems (ICEMS)*, pp. 1039–1045, 2015.

[20] R. Vargas, J. Rodriguez, C. A. Rojas, and M. Rivera, "Predictive control of an induction machine fed by a matrix converter with increased efficiency and reduced common-mode voltage," *IEEE Transactions on Energy Conversion*, Vol. 29, No. 2, pp. 473–485, 2014.

[21] A. J. Sguarezi Filho and E. Ruppert Filho, "Model-based predictive control applied to the doubly-fed induction generator direct power control," *IEEE Transactions on Sustainable Energy*, Vol. 3, No. 3, pp. 398–406, 2012.

[22] P. Kou, D. Liang, J. Li, L. Gao, and Q. Ze, "Finite-control-set model predictive control for DFIG wind turbines," *IEEE Transactions on Automation Science and Engineering*, Vol. 15, No. 3, pp. 1004–1013, 2018.

[23] A. S. Abdel-Khalik, M. I. Masoud, B. W. Williams, A. L. Mohamadein, and M. Ahmed, "Steady-state performance and stability analysis of mixed pole machines with electromechanical torque and rotor electric power to a shaft-mounted electrical load," *IEEE Transactions on Industrial Electronics*, Vol. 57, No. 1, pp. 22–34, 2010.

[24] S. Vazquez, J. Rodriguez, M. Rivera, L. G. Franquelo, and M. Norambuena, "Model predictive control for power converters and drives: Advances and trends," *IEEE Transactions on Industrial Electronics*, Vol. 64, No. 2, pp. 935–947, 2017.

[25] N. Mohan, *Power electronics: A first course*. Wiley, 2011.

R. Rezavandi was born in 1991, in Iran. He received his B.Sc. degree in Electrical Engineering from Razi University, Kermanshah, Iran, in 2013, and M.Sc. degree in Electrical Engineering from Iran University of Science and Technology (IUST), Tehran, Iran, in 2015. Since 2015, he has been cooperating with Electronics Research Center of IUST as a researcher. His research interests include predictive control, power electronics converters and motor drives.

D. A. Khaburi was born in 1965. He has received B.Sc. in Electronic Engineering, in 1990 from Sharif University of Technology, Tehran, Iran, and M.Sc. and Ph.D. in Electrical Engineering, from ENSEM, INPEL, Nancy, France in 1994 and 1998, respectively. Since January of 2000 he has been as a faculty member in Electrical Engineering Department of Iran University of Science Technology (IUST), where he is currently as an Associate Professor. He is also a member of Center Of Excellence for Power Systems Automation and Operation. His research interests are Power Electronics, Motor Drives and Digital Control.

M. Siami was born in Mazandaran, Iran, in 1986. He received the B.Sc. degree from Guilan University, Rasht, Iran, in 2009 and the M.Sc. degree from Babol (Noshirvani) University of Technology, Babol, Iran, in 2012, and the Ph.D. degree from Iran University of Science and Technology (IUST), Tehran, Iran, in 2017, all in Electrical Engineering. Since 2017 he is with Iran Power Generation, Transmission & Distribution Management Co. (TAVANIR), Tehran, Iran. His researh intrests include predictive control, power electronics and matrix converter.

M. Khosravi was born in Tehran, Iran, in 1993. He received the B.Sc. and M.Sc. degrees in Electrical Engineering from Iran University of Science and Technology (IUST), Tehran, Iran, in 2014 and 2016, respectively. He is currently pursuing the Ph.D. degree in Electrical Engineering at Iran University of Science and Technology (IUST). He is also a member of Iran's National Elites Foundation. His research interests include power electronic converter topologies and control strategies, renewable energy systems and electrical drives.

S. Heshmatian was born in Tehran, Iran, in 1992. He received the B.Sc. and M.Sc. degrees in Electrical Engineering from Iran University of Science and Technology (IUST), Tehran, Iran, in 2014 and 2016, respectively. His research interests include power electronic converter topologies and control strategies and renewable energy systems. He is currently cooperating with Electronics Research Center of IUST as a researcher.